Supplementary Information

Unraveling low-temperature structural and dielectric characteristics in lead-free bismuth halide perovskites

Naveen Kumar Tailor,[1,2] Rohit Kumar Rohj,[3] Krishanu Dey,[4] Samuel D. Stranks,[5,6] D. D. Sarma,[3] Soumitra Satapathi[1,2,*]

[1]Department of Physics, Indian Institute of Technology Roorkee, Roorkee 247667, India

[2]Center for Sustainable Energy, Indian Institute of Technology Roorkee, Roorkee 247667, India

[3]Solid State and Structural Chemistry Unit, Indian Institute of Science, Bengaluru 560012, India

[4]Clarendon Laboratory, Department of Physics, University of Oxford, Parks Road, Oxford OX1 3PU, United Kingdom

[5]Cavendish Laboratory, Department of Physics, University of Cambridge, JJ Thomson Avenue, Cambridge CB3 0HE, United Kingdom

[6]Department of Chemical Engineering & Biotechnology, University of Cambridge, Philippa Fawcett Drive, Cambridge CB3 0AS, United Kingdom

***Corresponding author: soumitra.satapathi@ph.iitr.ac.in**

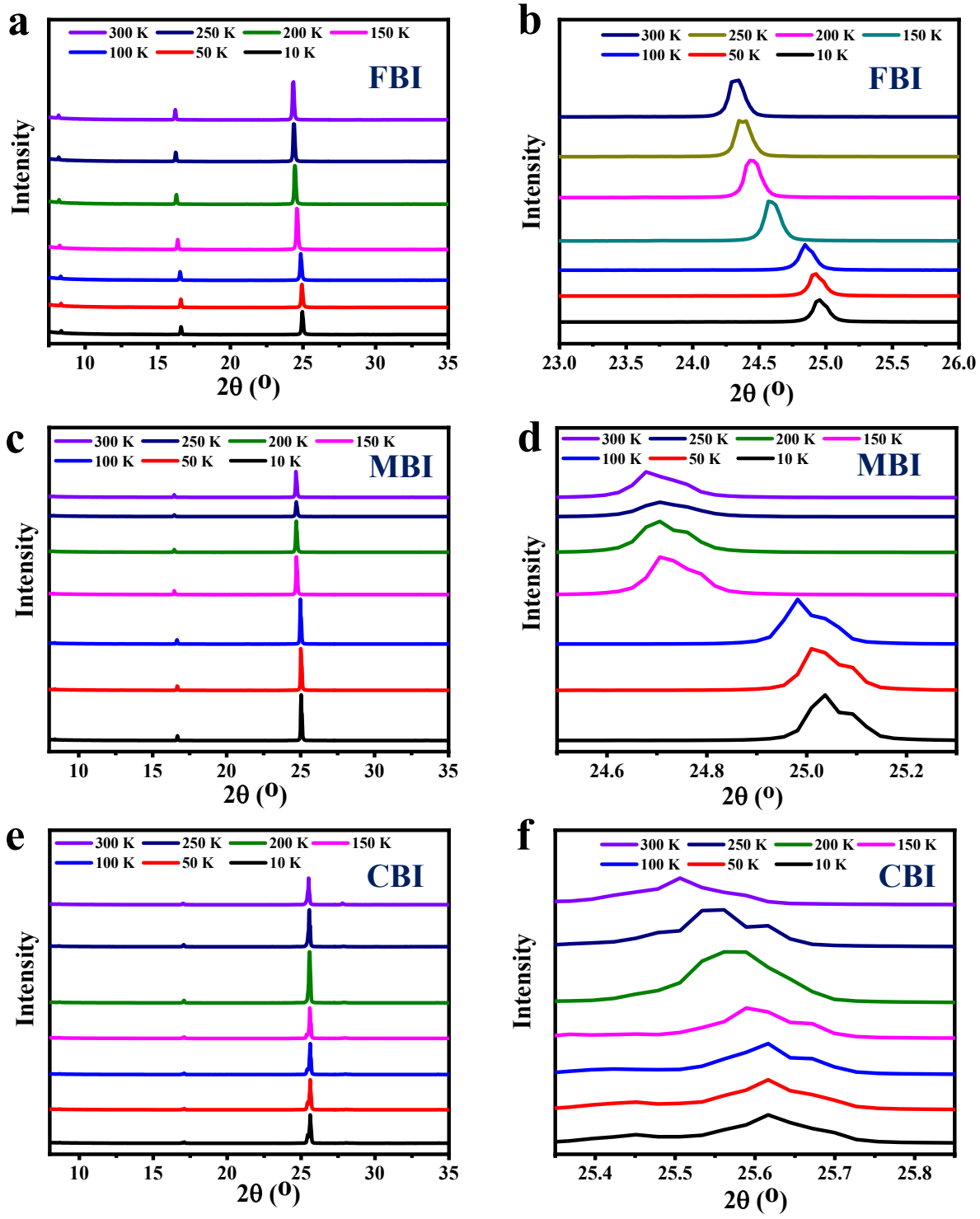

Figure S1. Powder XRD pattern of the $A_3Bi_2I_9$ [ABI; A = FA, MA, Cs] single crystals as a function of temperature. (a, d) FBI, (b, e) MBI, and (c, f) CBI crystals. The prominent peak is zoomed as (d) FBI, (e) MBI, and (f) CBI crystals.

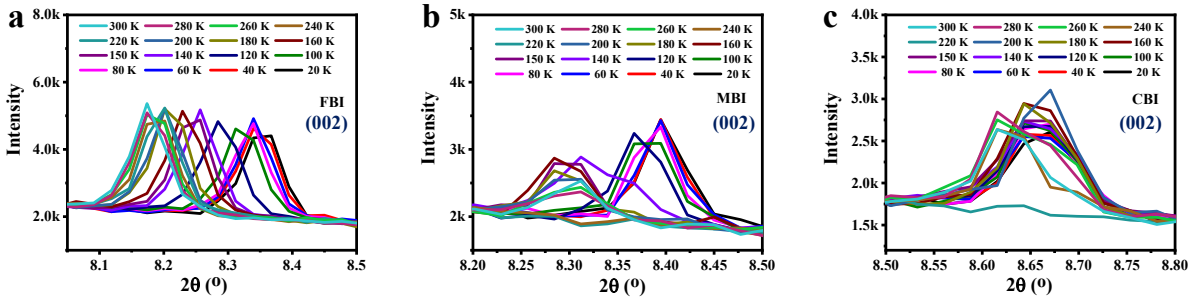

Figure S2. XRD Peak position variation as a function of temperature of the ABI (A = FA, MA, Cs) single crystals. The prominent peaks are zoomed as (002) plane of (a) FBI, (b) MBI, and (c) CBI crystals.

In the XRD pattern of MBI, we have observed that XRD peak splits at 140 K which is signature of phase transition. We observed that for (002) plane peak splitting is less visible, for (004) plane peak splits with similar intensity and for (006) plane, higher angle peak have slightly higher intensity than the lower angle peak (**Figure S3**). The intensity value and their ration is as follows:

Plane	Peak 1	Peak 2	Ratio
(004)	4921	4876	1.009
(006)	36873	49561	0.743

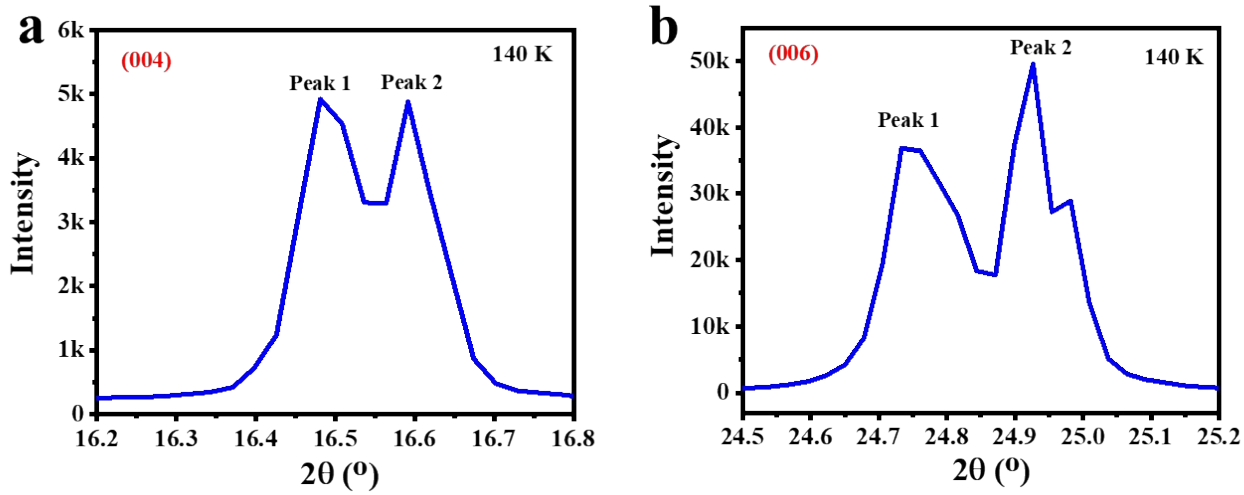

Figure S3. (a) Zoomed version of XRD at 140 K for (004) plane and (006) plane showing the peak splitting.

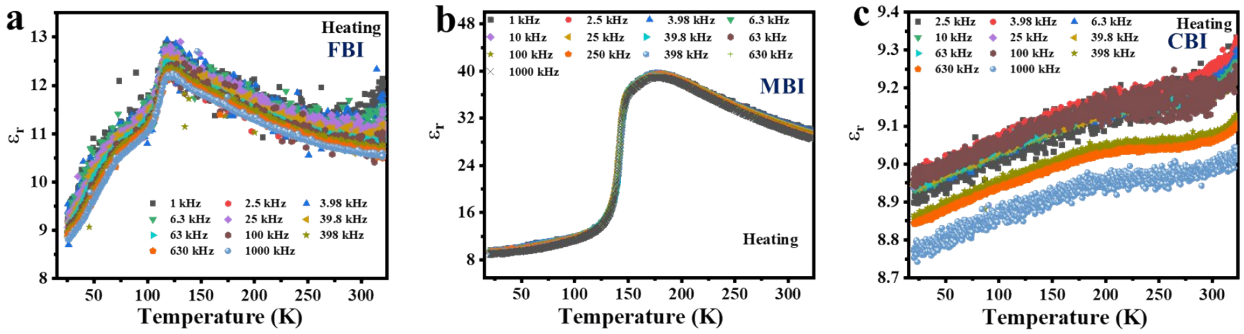

Figure S4. Dielectric constant as a function of temperature for ABI (A = FA, MA, Cs) single crystals measured at different frequencies while heating. The measurement was performed on pellets of these crystals fabricated by grinding these crystals. (a) FBI, (b) MBI, (c) CBI.

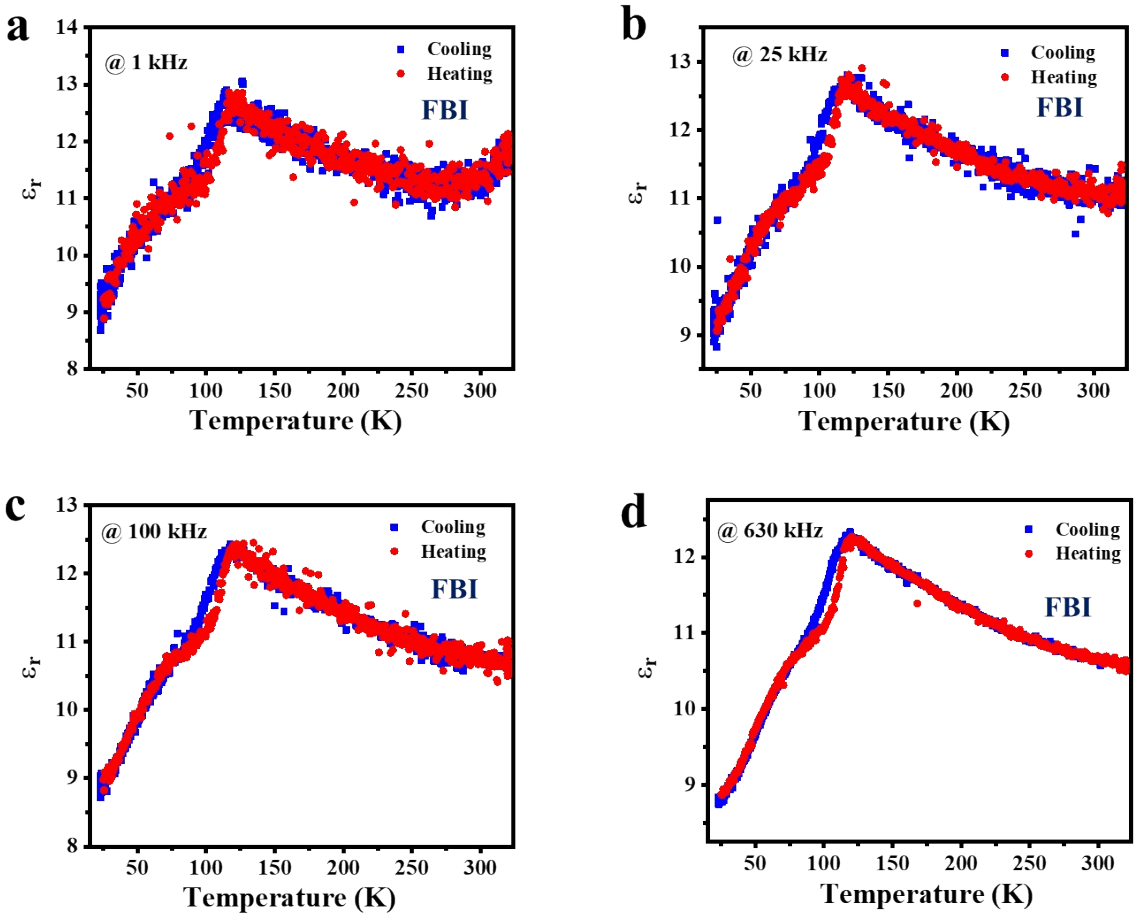

Figure S5. The dielectric constant as a function of temperature measured in cycle (cooling and heating) for FBI crystal. (a) 1 kHz, (b) 25 kHz, (c) 100 kHz, and (d) 630 kHz.

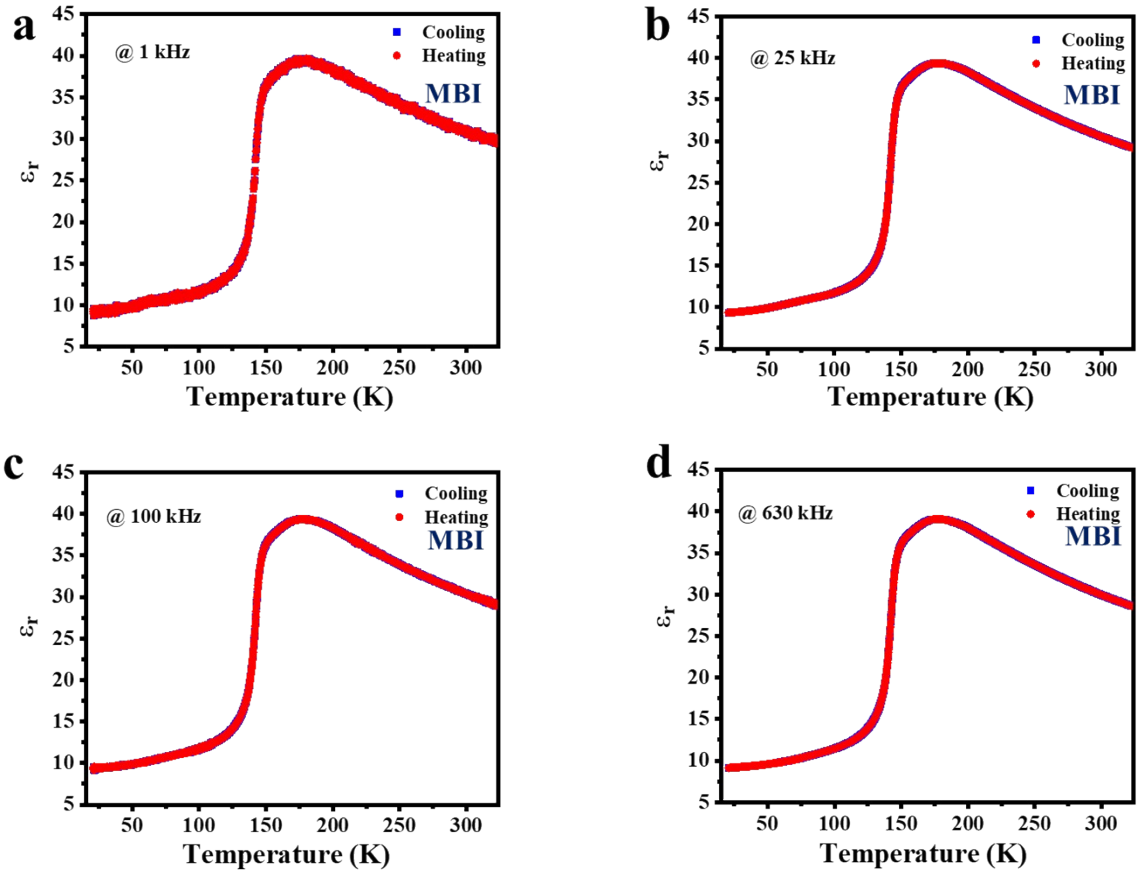

Figure S6. The dielectric constant as a function of temperature measured in cycle (cooling and heating) for MBI crystal. (a) 1 kHz, (b) 25 kHz, (c) 100 kHz, and (d) 630 kHz.

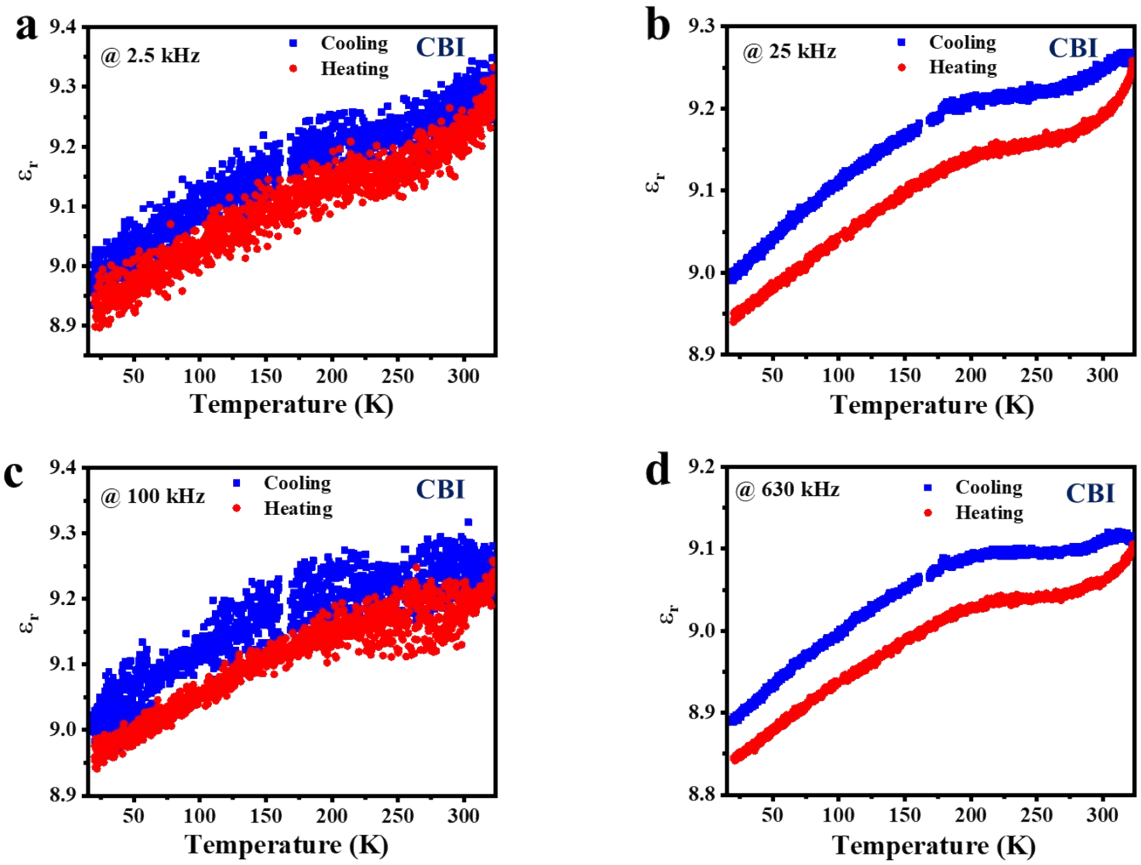

Figure S7. The dielectric constant as a function of temperature measured in cycle (cooling and heating) for CBI crystal. (a) 1 kHz, (b) 25 kHz, (c) 100 kHz, and (d) 630 kHz.

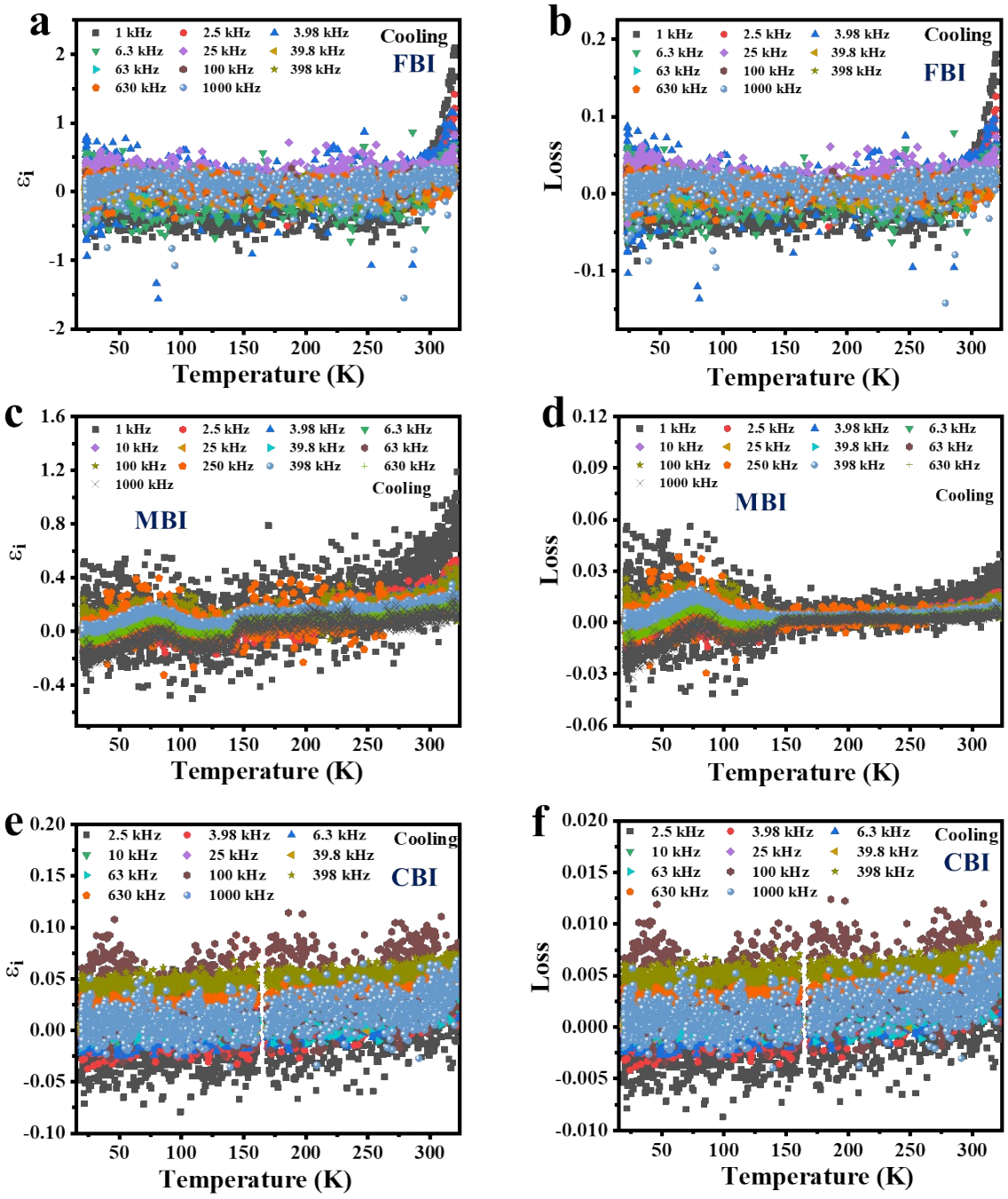

Figure S8. Imaginary part of dielectric constant as a function of temperature for ABI (A = FA, MA, Cs) system measured at different frequencies while cooling. (a) FBI, (c) MBI, (e) CBI. Dielectric loss as a function of temperature in same conditions. (b) FBI, (d) MBI, (f) CBI.

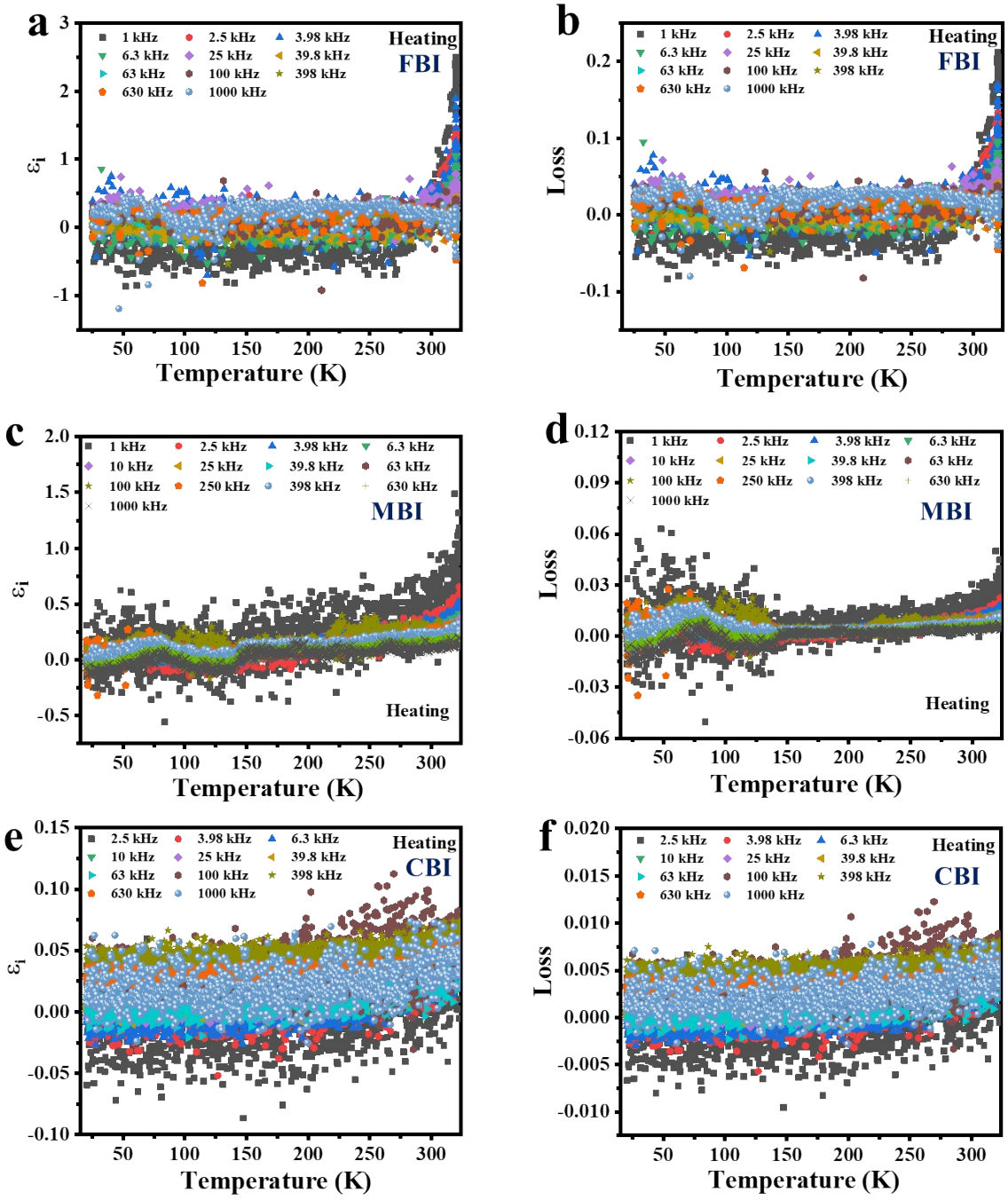

Figure S9. Imaginary part of dielectric constant as a function of temperature for ABI (A = FA, MA, Cs) system measured at different frequencies while heating. (a) FBI, (c) MBI, (e) CBI. Dielectric loss as a function of temperature in same conditions. (b) FBI, (d) MBI, (f) CBI.

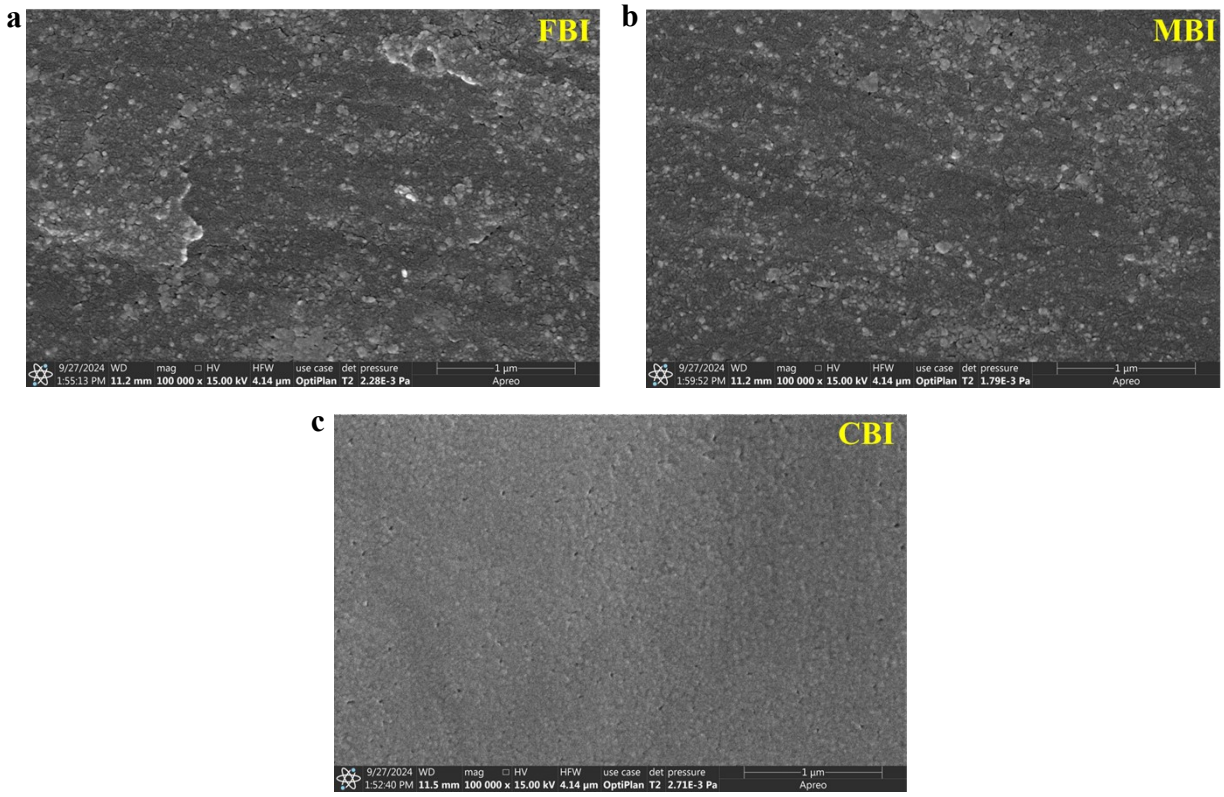

Figure S10. Morphology images of fabricated pellets (a) FBI, (b) MBI, (c) CBI.

Supplementary Note 1.

Regarding the influence of pore size and quantity, the dielectric measurements were performed on pelletized samples, where porosity can indeed affect the dielectric permittivity. Firstly, the pellets used for the dielectric measurements were fabricated under high-pressure conditions to ensure densification, which significantly minimizes the presence of pores. Thin pellets were specifically employed for these measurements, as thinner samples are generally associated with lower porosity due to the uniform distribution of pressure during the fabrication process. This approach inherently reduces the influence of pores on the dielectric response. To further substantiate this, we have obtained Scanning Electron Microscopy (SEM) images of the pellet surface (Figure S10). The SEM analysis reveals that the surface of the pellets contains very few pores, confirming that the porosity is very less. Based on this experimental evidence, we can reasonably conclude that the convergence of dielectric constants at lower temperatures is not primarily driven by sample inhomogeneity or porosity effects.

Additionally, we would like to highlight that the observed trend in the dielectric constant is consistent with previously reported studies (Inorg. Chem. 2017, 56, 1, 33–41; J. Mater. Chem. C, 2019, 7, 3003-3014). In the case of CBI, only a minor variation in dielectric constant with temperature was observed. This indicates that the dielectric properties are strongly influenced by

the rotational dynamics of the organic cations, as discussed in the manuscript. At lower temperatures, the rotational freedom of the organic cations, particularly for systems like MBI and FBI, becomes restricted, leading to a freezing of the dipole moments. As a result, the dielectric constant decreases and converges to a similar range for all three materials. This convergence further suggests that the inorganic $[Bi_2I_9]^{3-}$ octahedral cage plays a negligible role in the dielectric variation with temperature, reinforcing the idea that the primary contribution to the dielectric properties originates from the dynamics of the A-site organic cations.